The adsorption of Ba on Ag(111)

1993 J. Phys.: Condens. Matter 5 5411

(http://iopscience.iop.org/0953-8984/5/31/006)

J. Phys.: Condens. Matter 5 (1993) 5411–5428. Printed in the UK

The adsorption of Ba on Ag(111)

U van Slooten, W R Koppers, A Bot†, H M van Pinxteren, A M C Moutinho‡, J W M Frenken and A W Kleyn

Association EURATOM-FOM, FOM-Institute for Atomic and Molecular Physics, Kruislaan 407, 1098 SJ Amsterdam, The Netherlands

Received 5 April 1993

Abstract. The growth behaviour of barium on silver(111) at room temperature is investigated by AES, XPS, MEIS, TDS, work function measurements and by monitoring the secondary-electron-emission crystal current. It is shown that, for low coverage, initially a 2D monolayer is formed. For higher coverages the overlayer formed resembles a structure formed by Poisson or Stranski–Krastanov growth with small islands. As evaporation continues the islands become very large or the sticking coefficient drops to zero. Annealing the Ag with more than one monolayer of Ba on top shows a large work function decrease of 0.6 eV to an unusually low value of 1.9 eV. The lowering of the work function can partly be explained by the formation of large clusters. Coadsorption experiments with H_2 indicate that the H_2 sticking coefficient on Ba/Ag(111) is constant and that the H_2 adsorbs dissociatively into one binding state. From the experiments an inelastic mean free path of 11 ± 1 Å for 351 eV electrons and 17 ± 1 Å for 1113 eV and 1119 eV electrons is deduced.

1. Introduction

The production of negative hydrogen ions at low-work-function (low-WF) surfaces has been a major research topic over the last decades. Much of the interest in this type of research originates from the production of high-energy intense neutral beams, which are necessary for plasma heating, current drive and diagnostic purposes in next generation Tokamaks [1]. In order to produce these high-energy intense neutral H beams, negative ions are accelerated to the required energy and subsequently neutralized. Presently, two types of source are under study to produce these negative ions. In a so-called volume source H^- is formed via vibrational excitation of H_2 molecules by fast electrons, followed by dissociative attachment by slow electrons [2]. In a surface conversion source, H^- is formed by the conversion of positive ions into negative ions at a low-WF surface via resonant charge exchange [3]. As a converter material barium is superior to caesium, a material which has been used in the past. Although the production rates of negative ions are comparable at both surfaces [4], Ba has a lower vapour pressure, a lower reactivity in air and can be machined and manufactured more easily.

Besides the use of Ba in negative ion sources, Ba finds application as a cathode material [5]. In high-emission cathodes the essential feature is a monolayer of BaO adsorbed on a metal such as tungsten. In a simple picture, the Ba loses its valence electron to the metal [6]. The resulting positive ion induces an image charge in the substrate, producing dipoles

† Present address: Unilever Research Laboratorium, PO Box 114, 3130 AC Vlaardingen, The Netherlands.

‡ Permanent address: GIDS—Departamento de Física, Faculdade de Ciências e Technologia, Universidade Nova de Lisboa, 2825 Monte da Caparica, Portugal.

0953-8984/93/315411+18$07.50

which lower the WF, thus enhancing the electron emission yield. The O is thought to be positioned in between the Ba and the substrate, thus increasing the bond length and the dipole moment.

Until now surface science studies under UHV conditions concerning the conversion of positive into negative ions at Ba surfaces have only been performed by Van Os *et al* [4]. In contrast H^- formation at Cs has been studied extensively (see, e.g., [7]). However, before studying the processes leading to H^-, knowledge about the Ba surface itself is indispensable. Since Ba single crystals are commercially not available, the Ba surface has to be produced via the adsorption of Ba onto a substrate material. Silver is chosen as substrate material because it is relatively easy to prepare and clean.

If atoms are adsorbed on top of a substrate there are several modes via which growth can proceed [8]. In case of very rapid diffusion, equilibrium on the surface is achieved and the different growth mechanisms to be discussed are the result of a balance between substrate surface energy, adsorbate surface energy and the interfacial energy [9]. Only if detailed knowledge is available of each of these energies can predictions be made concerning the growth. However, for most systems the interfacial energy especially is not known accurately. Furthermore, if the diffusion of the adsorbates is slow, the grown structures will not attain surface equilibrium and the structure will depend more on the kinetics of the adsorption process.

In the rapid-diffusion case, in principle three different growth mechanisms are distinguished [8]. First there is Frank–van der Merwe (FM) growth. In this growth model the adsorbates grow multilayers in a monolayer-by-monolayer fashion. In contrast to FM growth is Volmer–Weber (VW) growth. Here three-dimensional clusters are formed on top of the surface. The third model is Stranski–Krastanov (SK) growth. In this model the growth is initially FM; later this changes to VW. While FM and SK growth have been observed for a large number of systems, VW growth is only observed for a limited number of systems [8].

The three above-mentioned basic growth models have in common that the mobility of the adsorbates is very high. For systems with a much smaller mobility two additional growth modes can be distinguished [8]. The simultaneous multilayer (SM) or Poisson growth model assumes that the surface mobility of the adsorbate atoms is negligible; the particles stick only at the position where they hit the surface. The monolayer plus simultaneous multilayers (MSM) model combines both diffusion regimes. After the formation of a monolayer (rapid surface diffusion) the growth changes, leading to a Poisson distribution without any diffusion.

Here we have to note that all of the five growth models mentioned neglect the possibility of alloying and diffusion of the adsorbates into the substrate. Furthermore, in all models the sticking coefficient is supposed to have a non-changing finite value. However, for many systems a decrease in sticking coefficient is observed as the growth proceeds until finally no more adsorbates stick on the surface (see, e.g., [10–13]).

In this paper we present the growth behaviour of Ba on an Ag(111) surface as revealed by Auger electron spectroscopy (AES), x-ray photoelectron spectroscopy (XPS), secondary-electron-emission crystal current (SEECC), thermal desorption spectroscopy (TDS), WF measurements and medium-energy ion scattering (MEIS). Furthermore, we investigate the stability upon heating of the adsorbed layer and the effect annealing has on the morphology and the WF of the adsorbate substrate system. Because the negative ion formation in a surface conversion source takes place at a relatively high H_2 pressure ($p \simeq 2 \times 10^{-4}$ mbar) [3] some coadsorption experiments with H_2 are also carried out.

2. Experimental details

The experimental set-up used in most of the experiments is described in detail elsewhere [14]. Briefly, it consists of a UHV chamber with base pressure in the low 10^{-11} mbar region. To reach this pressure the system is pumped by two turbo pumps in series (500 and 50 l s^{-1} respectively) and a liquid nitrogen cooled titanium sublimation pump. The residual gas almost solely consists of H_2, as checked by a quadrupole mass spectrometer (QMS) (Balzers 420). During experiments the pressure was always below 2×10^{-10} mbar. The QMS is also used to monitor desorbed species in the TDS experiments; in these experiments the crystal is linearly heated (11 K s^{-1}) by means of electron bombardment. Besides the QMS, facilities for the characterization of the clean and adsorbate covered crystal are mounted. For the AES experiments the sample is irradiated by 1720 eV electrons; secondary electrons are analysed by a cylindrical mirror analyser (CMA) (Riber). The XPS data are produced by aiming x-rays with an energy of 1486.6 eV produced by an aluminium Kα source (VG, XR 3) at the crystal. Emitted electrons are analysed with a hemispherical analyser (VG, CLAM 2) with the pass energy set at 20 eV. For the clean Ag(111) surface the FWHM for the Ag 3d doublet thus measured is 1.1 eV. The energy scale is calibrated using the Ag $3d_{5/2}$ level at 367.9 eV [15]. WF changes are monitored by a Kelvin probe with an untreated gold reference surface (Delta-Phi, Jülich). For the SEECC experiments the crystal current (drain current to earth during impingement of the Auger electron beam or the x-ray beam) is monitored with the help of a picoammeter.

The Ag(111) crystal is cut by spark erosion and mechanically polished. The misalignment of the (111) surface is smaller than 0.05° as determined by Laue diffraction. To clean the crystal a sputter source is mounted. The following cleaning procedure is applied: alternate hot sputtering at normal incidence (t = 15 min, 800 eV Ar^+, $I_{sputter} = 5 \times 10^{-6}$ A, $T_{crystal}$ = 573 K) followed by annealing (t = 15 min, $T_{crystal}$ = 673 K). The surface cleanliness is checked by AES and XPS which yields the result that the contamination level was below 1% of a monolayer. WF measurements are also used to determine the cleanliness.

The crystal is mounted on a rotatable manipulator, thus making it possible to position the crystal in front of all the surface analytical tools mentioned above. Moreover, the crystal can be positioned in front of a Ba wire disperser (SAES, getters) at a distance of approximately 2 cm. This dispenser is resistively heated by a current of about 5 A, thus producing a constant reproducible Ba flux. With help of the QMS, which showed a reasonable sensitivity for Ba, it is verified that only Ba is evaporated at this heating current. Besides the Ba getter a Cs dispenser is mounted. With this dispenser the WF curve for Cs adsorption on Ag(111) [10] previously published could be reproduced. This provided an absolute WF scale.

For the MEIS experiments another UHV system is used. This system is described extensively in the literature [16]. A 100.75 keV He^+ beam with an incident angle of 45° with respect to the surface is backscattered from clean and Ba covered samples. The scattered ions are detected over a 4° angular range around a total scattering angle of 109.0° using an electrostatic analyser with an angular resolution of 0.1° and an energy resolution $\Delta E/E$ of 9×10^{-4} [17]. All measurements are carried out in the same orientation of crystal geometry. From the measured ion yields absolute surface coverages can be determined [18]. The absolute ion yields are calibrated with the help of a silicon surface barrier detector or normalized to the height of the scattered signal for a random direction using tabulated values for the random stopping power [19]. This UHV system is also equipped with a Ba dispenser and a CMA thus making it possible to directly compare the results obtained in the two different UHV systems.

3. Results

The experimental results to be shown are divided into three subsections. First the results of the adsorption study of Ba on the Ag(111) crystal at room temperature is presented. The second part deals with the results obtained by annealing the crystal to elevated temperatures. In the last part the results of the coadsorption of Ba and H_2 are mentioned briefly.

3.1. Barium adsorption

Figure 1 shows three typical spectra obtained with MEIS. The backscattered He^+ ion yield is plotted as a function of the final energy of the scattered particles. The three spectra are taken for different Ba coverages present at the surface. For a clean Ag surface peak only one peak would be visible with its leading edge at an energy of k^2E_p, where k denotes the kinematic factor for an elastic collision ($k^2 = 0.906$ for Ag) [18] and E_p the primary beam energy of 100.75 keV. Since Ba is heavier than Ag the kinematic factor for Ba is larger ($k^2 = 0.925$), thus He^+ ions scattered from Ba appear at higher energies. For a Ba covered surface the ions scattered from the Ag suffer beside the elastic collision energy loss an extra energy loss due to the electronic stopping in the Ba overlayer [19]. The peak position of the Ag will shift to lower energies with increasing coverage.

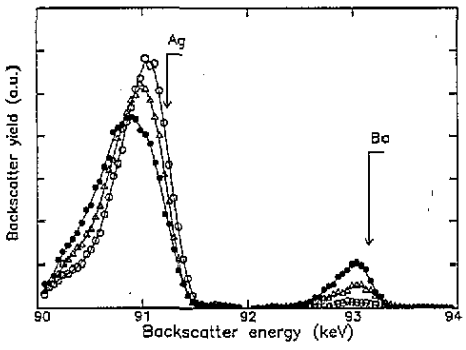

Figure 1. MEIS energy spectrum of backscattered ions for 0.08 (○), 0.2 (△) and 0.8 × 10^{15} (●) Ba adsorbates cm^{-2}. A 100.75 keV He^+ beam is scattered at an incident angle of 45°. The backscattered ions are energy analysed and collected over a 4° angular range centred around a total scattering angle of 109.0°. The arrows indicate the expected energy position for ions which are elastically backscattered from Ag and Ba surface atoms.

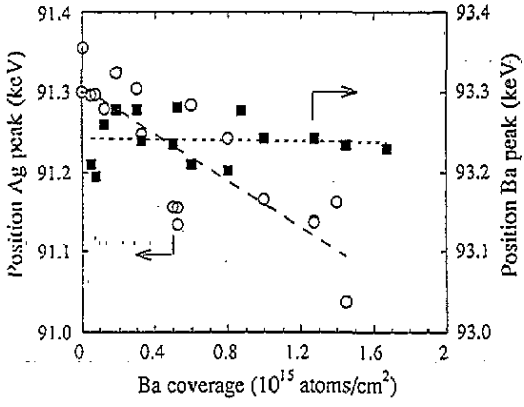

Figure 2. Energy position of the leading edge of the MEIS spectra of Ag (○) and Ba (■) as a function of Ba coverage. The absolute coverages are obtained by integration of the MEIS spectra.

Because of the additional energy loss due to the electronic stopping, it is clear that the positions of the leading edges of the Ba and Ag peaks are very sensitive to the actual depth position of adsorbate and substrate [18]. Figure 2 shows the energy position of the leading edge as a function of the amount of adsorbed Ba as determined in the experiment [18]. The Ba position remains constant over the whole range, while the Ag edge moves continuously to lower energies.

Besides the position of the edge, the width of the edge can also yield information [20]. Variations in thickness of the adsorbate layer and mixing of adsorbate and substrate will increase the width of the substrate peak. Straggling in the adsorbate layer can also increase the width [19]. Figure 3 shows that the width of the Ba leading edge is constant for all Ba coverages. The width of the Ag leading edge remains constant until 0.6×10^{15} adsorbates cm^{-2} are present; after this the width increases linearly. To make this clearer in figure 3 the Ag data are presented in two ways. Besides the experimentally determined Ag widths, the widths are also shown after deconvolution with the clean Ag width.

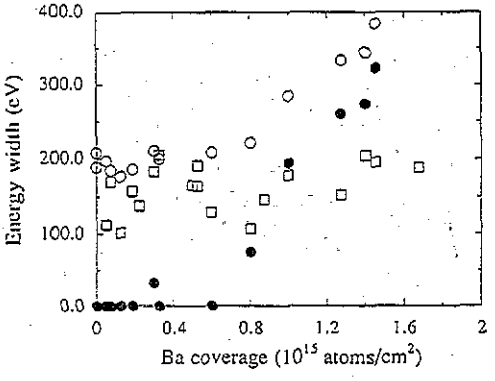

Figure 3. Width of the leading edge of the MEIS spectra for Ag (○) and Ba (□) as a function of Ba coverage. Also shown is the Ag width (●) after deconvolution with the Ag width for zero coverage. The absolute Ba coverages are obtained by integration of the MEIS spectra.

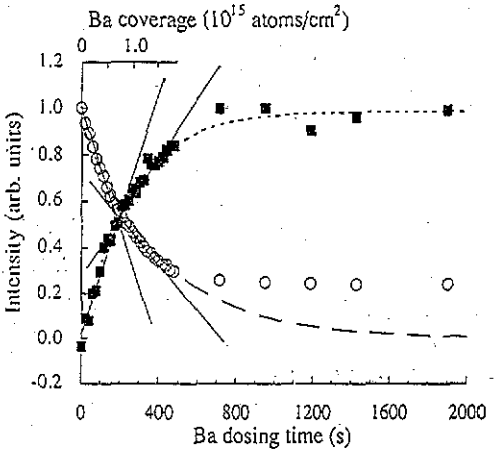

Figure 4. Ag (351 eV) (MNN) (○) and Ba (585 eV) (MNN) (■) AES peak-to-peak height as a function of Ba dosing time and coverage. The exponential curves and straight lines are discussed in section 4.

Since the MEIS experiments on one hand and all the other measurements on the other hand are done in two different experimental set-ups, Auger spectra which could be made at both set-ups are used to calibrate the experiments with respect to each other. From the comparison of the experiments it turns out that the sticking coefficient of Ba is constant up to a coverage of at least 1.8×10^{15} adsorbates cm^{-2}. Since no MEIS experiments are carried out at higher coverages, we cannot say anything concerning the sticking coefficient for higher coverages. In the AES measurements it turned out that the Ba source in the MEIS set-up was not entirely free of O contamination. For the adsorption study this was of minor importance.

In order to determine the growth mechanism for adsorbate atoms on top of a substrate AES has also proven to be a valuable technique. Following the intensities of both the adsorbate and the substrate as a function of dosing time provides much information concerning the morphology of the system under study [8]. Figure 4 shows the peak-to-peak heights in a differential AES spectrum of the Ag 351 eV (MNN) and the Ba 585 eV (MNN) line as a function of dosing time and coverage (up to 1.8×10^{15} adsorbates cm^{-2}). Initially the Ba line intensity increases more or less linearly before it levels off to a certain level. The Ag line shows the opposite behaviour; after an initial sharp decrease it converges

to a constant level. It is noteworthy that the Ag signal does not decrease to zero, even for long dosing times. The exponential curves and lines drawn in the figure will be referred to in the discussion section (4.1) of this paper.

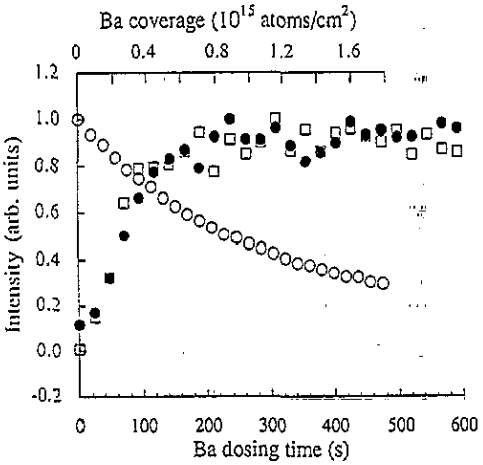

Figure 5. Ag (351 eV) (○), Ba (57 eV) (□) and Ba (73 eV) (●) AES peak-to-peak height as a function of Ba dosing time and coverage. Note the change in scale with respect to figure 4.

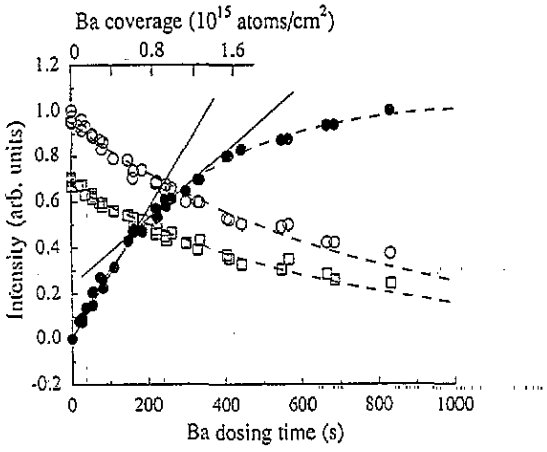

Figure 6. Ag $3d_{3/2}$ (373.9 eV) (□), Ag $3d_{5/2}$ (367.9 eV) (○) and Ba $3d_{5/2}$ (780.6 eV) (●) XPS core level intensities as a function of Ba dosing time and coverage. The exponential curves and straight lines are discussed in section 4.

In figure 5 the intensities of two low-energy Ba lines at 57 eV and 73 eV are shown beside the Ag 351 eV line already shown in figure 4. Please note the change in scale. The levelling of the Ba lines to a constant level is much faster than for the Ag line. This can easily be understood in terms of the inelastic mean free path (IMFP) of the escaping electrons, which is much smaller for the low-energy Ba lines [21].

Like AES, XPS is a technique providing information about elemental composition of the surface region, although the surface sensitivity is generally less, since the electrons detected have a higher energy and thus an increased sampling depth [21]. Besides composition, depth and growth information, XPS can give information concerning the chemical environment via the energy position and the width of the detected lines. Figure 6 shows XPS results: the variation of the Ba $3d_{5/2}$ ($E_{binding} = 780.6$ eV), Ag $3d_{3/2}$ (373.9 eV) and Ag $3d_{5/2}$ (367.9 eV) line intensities is monitored as a function of dosing time and coverage. The spectra look like those of figure 4, although the constant level to which the Ag 3d lines merge is higher. This is due to the increased sampling depth in the XPS experiments: since the kinetic energy of the emitted electrons is higher (1113 and 1119 eV) the IMFP is larger [21]. The positions of the peaks only shift slightly upon Ba adsorption. The Ag $3d_{3/2}$ and Ag $3d_{5/2}$ shift approximately linearly with Ba coverage from 373.9 and 367.9 eV to a higher binding energy by 0.4 eV over the whole dosing range. The relative positions of the two Ag lines do not shift but remain constant at 6.0 eV. In contrast to the Ag lines, the Ba line shift from 780.6 eV to a lower binding energy. After an initial decrease of 0.6 eV in the first 300 s (1.1×10^{15} adsorbates cm^{-2}) the line position remains more or less constant.

Monitoring the width of the Ag and Ba lines as a function of dosing time and coverage gives a dependence as shown in figure 7. The monitored widths are not corrected for the analyser resolution of 1.0 eV. The Ag line widths increase only slightly from 1.1 eV to

1.2 eV upon Ba adsorption, while the increase for the Ba line is much larger. During the first 220 s (0.8×10^{15} adsorbates cm^{-2}) the width increases more or less linearly from 1.3 to 2.0 eV and then decreases slightly to 1.8 eV.

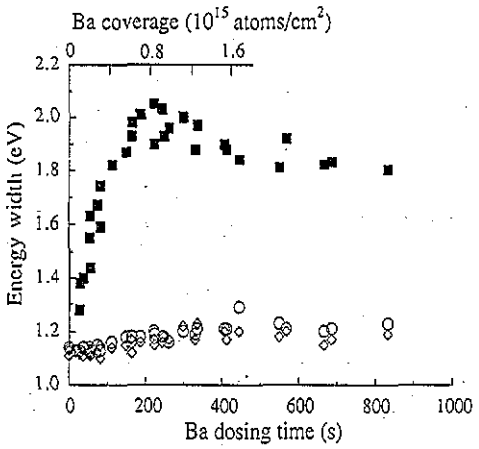

Figure 7. Ag $3d_{3/2}$ (◇), Ag $3d_{5/2}$ (○) and Ba $3d_{5/2}$ (■) XPS core level widths as a function of Ba dosing time and coverage.

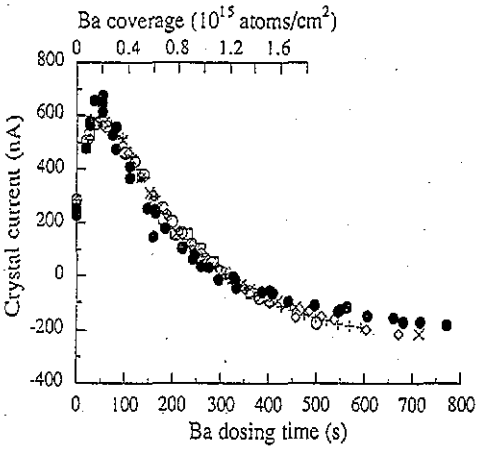

Figure 8. Measured crystal current as a function of Ba dosing time and coverage. The five different open symbols denote five different experiments performed with the Auger electron gun. The filled symbols are currents measured using the photon beam. In order to make a direct comparison with the electron induced SEECC possible, a constant current is subtracted for the x-ray induced SEECC curve. This offset accounts for the absence of a current due to the incident electrons in the x-ray induced SEECC curve.

Figure 8 shows the variation of the adsorbed drain current to ground via the crystal as a function of dosing time and coverage. Earlier work has shown that measuring the SEECC is a relatively easy technique to look at adsorbate growth and to monitor changes in WF and in electron density of the crystal [8, 10, 12, 22]. In the figure five different adsorption experiments monitored with the Auger electron gun are depicted, showing the reproducibility of the obtained currents. Moreover, similar data are obtained when the x-ray source is used. To enable a direct comparison with the electron induced SEECC an offset is added to the x-ray induced data. This offset accounts for the absence of a current due to the incident electrons in the x-ray induced SEECC data. Subsequently, the data are scaled to the electron induced data. Since the number of emitted electrons is a function of the incident energy, it is not surprising that the x-ray induced data are not identical to the electron induced data, nevertheless they look the same. Measuring the crystal current is a handy additional method to calibrate the different experimental techniques with respect to each other.

If the WF is measured, the spectra obtained upon dosing look very similar to the alkali metal WF curves (see, e.g., [10, 11, 23]) and to curves obtained for Ba adsorbed on other metals (see, e.g., [24]–[26]). Figure 9 shows that after an initial sharp linear decrease the WF levels off and passes through a minimum about 0.15 ± 0.02 eV deep and then increases to a value of 2.5 ± 0.1 eV, which is close to the value for bulk Ba. The error of 0.1 eV is mainly due to the calibration of our Kelvin probe, which only measures WF differences, and is calibrated to the Cs/Ag(111) WF curve [10]. The experimental error is only 0.02 eV.

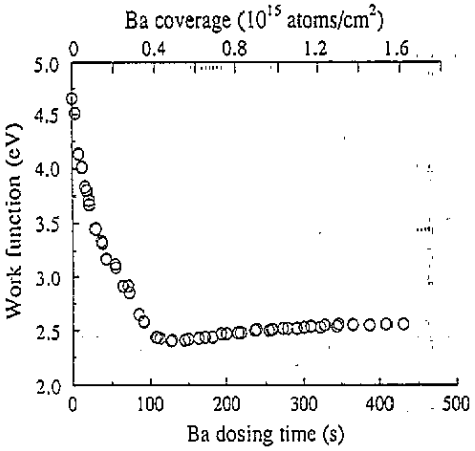

Figure 9. WF of the crystal as a function of Ba dosing time and coverage.

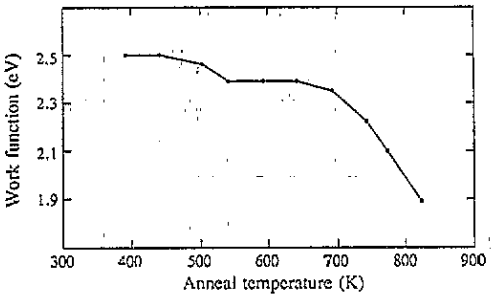

Figure 10. WF of an Ag(111) crystal dosed with Ba for 400 s (1.5×10^{15} adsorbates cm^{-2}) as a function of annealing temperature. The data are taken after cooling the crystal to room temperature.

3.2. Annealing

In order to obtain some information concerning the thermal stability of the adsorbed layer, the crystal is flashed to a certain temperature and subsequently cooled down. First, the effect of this annealing on the WF is measured. If a small amount of Ba (equivalent to 140 s dosing time or 0.5×10^{15} adsorbates cm^{-2}) is deposited, the WF remains constant in the temperature range up to 820 K. However, if the amount of adsorbed Ba is increased there is a large effect on the WF. In figure 10 the change in WF after annealing is shown; the amount of Ba present at the surface results from a 400 s dose (1.5×10^{15} adsorbates cm^{-2}). At first, a small WF decrease of about 0.1 eV is observed between 300 and 550 K. An even higher WF decrease is observed between 620 and 820 K. The WF obtained after annealing to 820 K is as low as 1.9 ± 0.1 eV. Unfortunately, it was not possible to anneal at even higher temperatures due to the low sublimation temperature of Ag [27].

The current measured by the SEECC measurements is also greatly influenced by annealing. During the annealing of the crystal with a Ba coverage equivalent to a 500 s dose ($\sim 1.9 \times 10^{15}$ adsorbates cm^{-2}) the signal changes from -150 nA to $+10$ nA indicating that it becomes easier for the electrons to escape from the solid into the vacuum.

Figure 11 shows the changes in XPS line intensities upon annealing. These data points are obtained after a 680 s ($> 1.8 \times 10^{15}$ adsorbates cm^{-2}) Ba dose. At a temperature between 500 and 550 K the Ba intensity suddenly drops while the Ag line intensities increase. If only small amounts ($< 0.6 \times 10^{15}$ adsorbates cm^{-2}) of Ba are deposited no change in line intensities is observed upon annealing. Contamination of the adsorbed layer with O also inhibits the change in line intensities.

Shown in figure 12 as a function of dosing time are the line intensities before and after annealing. As can be seen in the figure, the change in line intensities becomes larger as more Ba is present at the surface. For a small dose no change is observed, but for the largest dose the change is as large as 40%. It is noteworthy that for all higher doses, the Ba line intensity after the anneal is the same. This also holds for the Ag line intensities. The final line intensities correspond to the intensities obtained after a dose of 300 s (1.1×10^{15} adsorbates cm^{-2}).

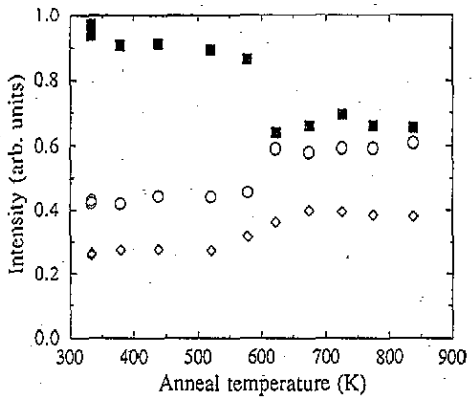

Figure 11. Ag $3d_{3/2}$ (◇), Ag $3d_{5/2}$ (○) and Ba $3d_{5/2}$ (■) XPS core level intensities as a function of anneal temperature. The experiment is performed on an Ag(111) crystal dosed with Ba for 680 s (> 1.8×10^{15} adsorbates cm^{-2}).

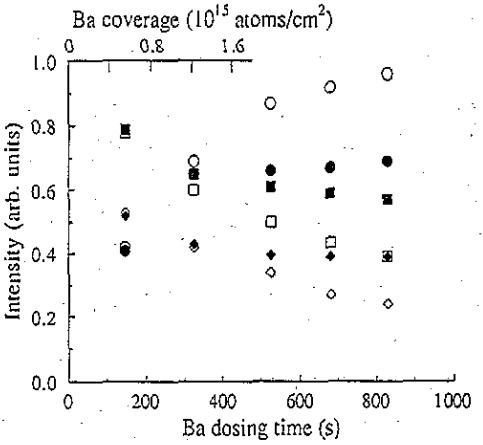

Figure 12. Intensity of the Ag $3d_{3/2}$ (□,■), Ag $3d_{5/2}$ (◇,◆) and Ba $3d_{5/2}$ (○,●) XPS core level intensities before and after annealing the crystal above 600 K as a function of Ba dosing time. The open symbols double the intensities before and the filled symbols after annealing.

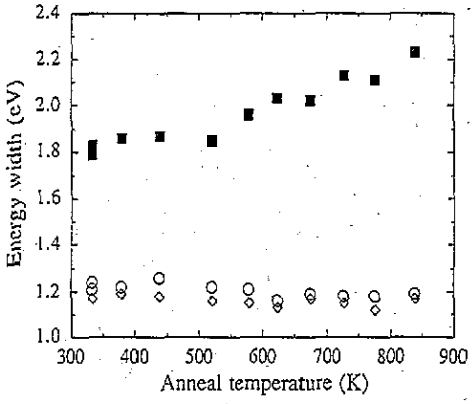

Figure 13. Ag $3d_{3/2}$ (◇), Ag $3d_{5/2}$ (○) and Ba $3d_{5/2}$ (■) XPS core level widths as a function of anneal temperature. The experiment is performed on an Ag(111) crystal dosed with Ba for 680 s (> 1.8×10^{15} adsorbates cm^{-2}).

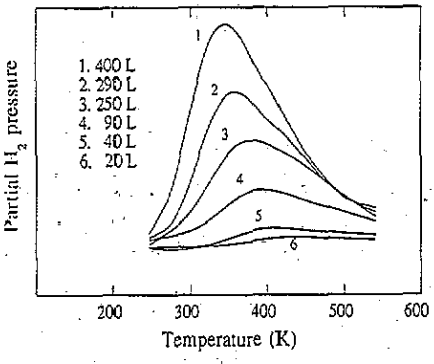

Figure 14. Thermal desorption spectra of H_2 from a preannealed Ba/Ag(111) surface for different experiments. The spectra are recorded using a heating rate of 11 K s^{-1}.

The XPS peak positions of all three monitored lines do not change within the experimental error. However, the width of Ba line increase for the high Ba doses. As is shown in figure 13, at the transition temperature of figure 11 the width also increases to the value obtained after a dose of 300 s (1.1×10^{15} adsorbates cm^{-2}). The amount of Ba in figures 11 and 13 is the same. For higher anneal temperatures the line width is increased even more. In contrast the Ag lines do not show any broadening. At this point it is wise to note that at the transition temperature the WF is also decreased to the value for a dose of 300 s (1.1×10^{15} adsorbates cm^{-2}).

From TDS experiments it turned out that during the annealing no Ba is desorbed. The total amount of Ba on the crystal remains constant.

Annealing deliberately oxidized Ba overlayers did not result in any change in intensities and widths, indicating that the oxidized layer is much more stable. Because of this we cannot extract information about changes in the morphology of a clean Ba layer upon annealing in the MEIS experiments, since in these experiments there was always some O contamination present.

3.3. Coadsorption of barium and hydrogen

Before studying the coadsorption of Ba and H_2 we verified using TDS that H_2 does not indeed stick on Ag(111) [28].

Dosing H_2 on a Ba covered Ag(111) crystal (400 s dose or 1.5×10^{15} adsorbates cm^{-2}) lowers the WF slightly by 0.02 eV. For this case no changes in line positions or line widths are observed in XPS.

Because the XPS results suggest changes in the Ba overlayer upon annealing the coadsorption experiments combined with TDS are carried out only on annealed samples. Figure 14 shows TDS spectra for different amounts of H_2 coadsorbed on the Ba/Ag(111) system. The amount of Ba present on the surface before annealing is equivalent to a dosing time of 400 s (1.5×10^{15} adsorbates cm^{-2}). In all spectra one peak can be identified, which shifts to lower temperatures as the H_2 dose is increased. Analysis of the amount of desorbed H_2 shows that the sticking coefficient is equal for all spectra. In XPS the line widths and line positions show no variations within the experimental error.

4. Discussion

4.1. Barium growth

Some clues concerning the morphology of Ba on Ag(111) can be given by MEIS. Analysing the position and width of the leading edge of the adsorbate and substrate signal gives information about which of the two elements is on top [18, 20]. If the Ba adsorbate stays on top, the position of the Ba edge will always be at the same energy position while the energy position of the Ag edge will move to lower energies. If the Ba is dissolved into the Ag crystal, the Ag edge will remain at the same position, the Ba peak will shift to lower energy and the width will increase. If the two materials mix, both leading edges remain at the same energy. For the Ba/Ag(111) case diffusion of the adsorbate into the substrate is very unlikely to happen. The phase diagram [29] shows that the two materials do not dissolve into each other. Furthermore the atomic diameter of Ba (4.34 Å) is simply too large to fit the Ba into the close packed Ag(111) (atomic diameter = 2.89 Å). Figure 2 shows that the Ba position remains constant and that the Ag position moves to lower energies as the amount of adsorbate increases. This directly shows that the Ba stays on top and does not mix with or dissolve into the Ag. From the linear change in position of the leading edge, an energy loss of about 150 eV per 10^{15} particles cm^{-2} is deduced. This is close to the 210 eV expected from tabulated stopping powers for He^+ ions travelling in bulk Ba [19].

Figure 3 shows that the width of the leading edge for Ba remains constant for all amounts of adsorbate present on the surface. The Ag width is constant until $0.60 \pm 0.05 \times 10^{15}$ particles cm^{-2} are adsorbed. From this coverage on, the width increases linearly, indicating a variance in layer thickness of the adsorbates. So, up to 0.6×10^{15} particles, Ba growth is restricted to the first layer because the layer thickness remains constant. This

indicates that the mobility of the Ba adsorbates is initially very large. This high mobility is observed also for Ba on W(011) [30]. In this system the diffusion coefficient is initially very large but decreases rapidly as the coverage is increased, leading to a strong limitation of the adatom mobility.

The $0.60 \pm 0.05 \times 10^{15}$ particles cm^{-2} found experimentally can be compared to two situations. First, the density in the closed packed (110) face of BCC Ba is equal to 0.56×10^{15} adsorbates cm^{-2}. This suggests that in the Ba overlayer on top of Ag the density of the closest packed face of Ba is reached. Since the lattice constants and crystal structures of the FCC Ag and the BCC Ba are different, the Ba would be incommensurate with the Ag substrate. This is observed also for Ba on W(011) [30, 31]. Although in this system initially commensurate structures are formed, these structures become incommensurate as the Ba density increases. A second possibility is the formation of a hexagonal overlayer of Ba on Ag(111). Since the atomic diameters of Ba and Ag differ by a factor of 1.50 a commensurate hexagonal overlayer can be formed, which has a density of 0.61×10^{15} particles cm^{-2}. Out of the experiments we cannot deduce anything concerning superstructures at low coverages.

For adsorption beyond 0.6×10^{15} particles cm^{-2} the growth continues. From the MEIS results it is not completely clear how the growth proceeds after the formation of the first monolayer. From the linear increase in width of the leading edge of the Ag peak (cf. figure 3) it can be deduced that the structure formed above the first monolayer will show variations in thickness. However, it is not very likely that very high 3D structures are formed. On the basis of the MEIS results we can exclude the VW and SM growth models, simply because of the formation of a first full monolayer.

By analysing the AES and XPS adsorbate and substrate signals as a function of dosing time, information concerning the type of growth can be extracted [8]. For FM growth the adsorbate signal is initially expected to increase linearly upon dosing. The substrate signal decreases linearly due to the inelastic scattering of the electrons in the overlayer. The linear increase and decrease is expected to continue until the first monolayer is formed. Consecutively, the increase and decrease will continue again linearly but with a different slope. For VW type growth the adsorbate and substrate signal only vary a little. This is due to incomplete shielding of the substrate and the rapid increase in heights of the formed cluster, which implies a very high attenuation of the adsorbate signal. From this it follows that SK signals are characterized initially by linear variations which change into slow variations. As can easily be shown SM growth is characterized by exponential variations for the adsorbate and substrate signal. For the MSM growth linear variations are observed until the first monolayer is formed. Hereafter exponential variations are observed. In practice it is very difficult to distinguish between SM and MSM growth.

Analysing the variations depicted in figures 4, 5 and 6 in line intensities of the Ag and the Ba lines as a function of dosing time directly shows that these variations are too rapid to be explained by VW growth. This is in agreement with the MEIS experiments.

To determine which of the other growth mechanisms can explain our data we first fitted exponential curves through the data. As can be verified, all the Ba line intensity variations can be reproduced quite well assuming an exponential dependence, which is characteristic of SM or MSM growth. In contrast, the exponential fits are not able to reproduce the variations in intensities for the Ag lines. So, this contradicts SM or MSM growth. This inadequacy of the exponential fit is mainly due to the fact that the Ag line intensities do not drop to zero for long dosing times. Fitting an exponential curve, taking into account that the intensity does not vanish, improves the agreement between the fitted curve and the experimental data considerably, although the fit is still not as good as for the Ba lines. A possible explanation for this remaining intensity could be that not all of the surface is covered because, e.g.,

the Ba only starts growing in the vicinity of steps which act as nucleation centres. On the part that is covered, the Ba is then growing in a SM or MSM manner. This is however in contradiction with the MEIS experiments, which show that the whole Ag surface is covered by the adsorbate. On the basis of these arguments we can exclude perfect SM or MSM growth.

As mentioned earlier in the discussion, FM growth would ideally be very easy to recognize. Due to the change in slopes of the increase and decrease of the line intensities as the adsorbate commences to grow in consecutive layers, breaks in the signal as a function of dosing time can be observed. These breaks are most pronounced if multilayers are unstable and only one layer of adsorbates can be grown on the substrate; this is observed for many alkali systems (see, e.g., [10]–[13]). The sketched mode of growth where adsorbates start growing a second layer only when the first layer is completely filled is an idealized situation. Due to the finite surface mobility of adsorbates in most cases the growth in the second layer starts before the first layer is completely filled. This leads to a rounding of the distinct breaks for the ideal FM growth. In figures 4 and 6 straight lines are also fitted through the data points beside the already described exponential curves. These lines strongly suggest the formation of a first monolayer after a 160 s dose (0.6×10^{15} adsorbates cm^{-2}). Until then the amount of adsorbates increases more or less linearly, which is consistent with the MEIS observation that the sticking coefficient remains constant up to at least 1.8×10^{15} adsorbates cm^{-2}. A rounding of the kink is indeed observed, so we start growing on top of the first layer before the first one is completely filled. This implies that the diffusion coefficient at coverages around one monolayer is not very large. The atoms deposited on top of the not completely filled Ba layer do not have enough mobility to migrate to the existing vacancies and are not incorporated in the layer beneath. This is also observed for Ba adsorption on W(011) [30]. As mentioned in the experimental section, in the MEIS set-up AES experiments could also be performed. These data show that the formation of a first monolayer after a 160 s dose (0.6×10^{15} adsorbates cm^{-2}) is in very good agreement with the MEIS experiments.

Analysing the low-energy (57 and 73 eV) Ba lines shown in figure 5 also supports the formation of a first monolayer. The IMFP of the escaping electrons is apparently considerably smaller than the layer spacing of 4.35 Å [21]. So, at a coverage of one monolayer the signal of these energies is already nearly equal to the signal for a film of infinite thickness.

Now the question remains of what the growth mechanism is after the formation of the first monolayer. For FM growth a complete disappearance of the substrate signal is expected. However, the Ag 351 eV line for long doses seems to remain at a constant level, as can be verified in figure 4. So, the growth does not change, although it is possible that a second layer is formed. The constant level of figure 4 can be explained in two ways. The first way is by SK growth: clusters are formed which extend preferably in height and leave a part of the crystal uncovered. For very high coverages these clusters eventually will coalesce [32] which leads to a vanishing of the substrate signal. However, this coalescence of the clusters has not yet been observed for the doses applied in our experiments, which are limited to at most 2000 s.

The other way to explain the constant level is by a change in sticking coefficient which is not considered in any of the five models. As demonstrated up to coverages of at least 1.8×10^{15} adsorbates cm^{-2}, the sticking is constant. At higher coverage the sticking coefficient could, in principle, decrease and finally drop to zero. In that case the adsorbed layer formed would not necessarily show large height fluctuations and would resemble a structure of the MSM model most.

4.2. Inelastic mean free path

Out of the attenuation of the Ag lines at the formation of one monolayer an IMFP of electrons moving through a Ba overlayer can be extracted. The ratio between the signal intensity at one monolayer and the signal at a clean surface for FM growth is expected to be $\exp[-d/(\lambda \cos\beta)]$ [21]. In this formula λ denotes the IMFP, d the distance between the substrate and the adsorbate and $\cos\beta$ a geometrical factor due to the angle between detector and surface normal. For d the atomic diameter of Ba of 4.34 Å is taken while $\cos\beta$ for the AES experiments is equal to 0.74 and for the XPS experiments to 0.91. The values thus obtained for the IMFP are 11 ± 1 Å for 351 eV electrons and 17 ± 1 Å for 1113 and 1119 eV electrons. These values are in the expected range of the so-called universal curve [21] and agree reasonably well with values observed for other energies in the literature assuming a $\sqrt{E}$ dependence for the IMFP. Eyink *et al* [26] deduce from their experiments an IMFP of 6.4 Å for 170 eV electrons (Ba/W), Cotter *et al* [33] calculate a value of 13.6 Å for 707 eV electrons (BaO/MgO(001)) while Weijs *et al* [34] use 20 Å for 1396 eV electrons (Ba/Si(100)).

4.3. Work function

For the production of negative ions on surfaces the WF is one of the key parameters [7]. In principle the lower the WF the higher the negative ion yield. In figure 9 the WF is recorded as a function of dosing time for the Ba/Ag(111) system. The WF shows a curve which is very similar to the WF curves of alkalis on metal surfaces (see, e.g., [10], [11] and [23]). After an initial sharp decrease with increasing Ba coverage the WF lowering levels off until it passes through a minimum value after ~ 0.8 monolayer (130 s dose or 0.5×10^{15} adsorbates cm^{-2}) after which a small increase is observed. In the alkali metal studies the observed WF behaviour is normally described within the Gurney model [6], see also, e.g., [35]. The first adsorbed Ba atoms lose their valence electrons almost completely to the substrate. This results in an almost complete ionization of the adsorbate. As a consequence the WF lowers. As the amount of adsorbate increases the repulsive interaction of the formed dipoles leads to depolarization effects which causes the WF to level. At a monolayer coverage the formed bonds will have lost most of their ionic character and the layer will be nearly metallic. The WF approaches the bulk value of the substrate. Similar WF curves are also reported in the literature for Ba on W (see, e.g., [24] and [30]), Si [36] and Cu [25]. From the initial decrease of the WF a dipole moment of 8 ± 1 D is deduced.

4.4. Secondary electron emission crystal current

The XPS and AES experiments are calibrated with respect to each other by performing WF and SEECC measurements in both cases as discussed in connection with figure 8. That secondary electron currents can provide information concerning growth was recognized for the first time by Bartès-Labrousse and Rhead [22]. Later this technique was successfully applied in following the growth of alkalis upon surfaces [8, 10, 12]. The principle of the technique is based on the fact that most materials have a different electron emission coefficient δ. At the energies used in our experiments, $\delta > 1$ for most metals, while for the alkalis and the earth alkalis $\delta < 1$ [37]. So, for Ba adsorption on a metal surface the recorded current will decrease as the coverage increases. However, as can be observed in figure 8, the recorded current initially increases. This increase is easily explained by the initial decrease in WF upon Ba adsorption. Due to this decrease it is easier for the electrons to escape into the vacuum, which results in an increase in recorded current. The combination of the changing emission coefficient and the changing WF explains the observed curve qualitatively. The

maximum in the SEECC signal is recorded after ~ 0.3 monolayer (50 ± 5 s dosing time or 0.2×10^{15} particles cm^{-2}) which is also observed for other systems [10, 12, 22].

4.5. XPS line widths and positions

During the deposition of the Ba overlayer we also followed the positions of the monitored XPS lines. Although it is not the aim of this paper to elaborately discuss the precise mechanisms which cause the observed line shifts, we will make some brief comments. The Ag line position shifts to slightly higher binding energies. Similar shifts for the substrate are observed also by Fischer *et al* [38] for Ba adsorption on Pd, and by Weijs *et al* [34] for Ba on Si(100). However, this shift is not observed by Ayyoob and Hedge [39] who determined the XPS line position of Ba on an Ag foil. For Ba, Weijs *et al* [34] also observe a shift in the Ba 4d line to lower binding energies, similar to our experiments. Their interpretation of the observed line shifts may be valid for the present results as well and is a combination of two effects. First of all there is a decrease in effective ionization of the Ba adsorbates as the Ba coverage increases, which lower the binding energy. As described, this decrease in ionization is also responsible for the leveling of the WF. The second effect responsible for the line shift is a more effective shielding of the created core holes as the coverage increases.

Besides the exact line positions the width of the lines is also determined in the experiments (figure 7). The Ag line width only increases slightly upon deposition. This is not surprising, since the energy of the recorded electrons is so high that in the experiments a dominating contribution from the Ag bulk is always measured due to the large IMFP (17 ± 1 Å) of the recorded electrons. The Ba line width is thus much more sensitive to changes in the adsorbed layer. This width increases rapidly. This inhomogeneous line broadening can be interpreted as an increase in the number of different chemical environments around the Ba adsorbates. After 220 s dosing time (0.8×10^{15} adsorbates cm^{-2}), which corresponds to a coverage of more than one monolayer, the level width decreases slightly. The interpretation of the recorded changes is rather straightforward and supports the growth model described in section 4.1. Initially the number of environments increases, while beyond the first monolayer the additional adsorbates all have the same environment. The decrease after 220 s is due to the decrease in ionization of the bindings between adsorbate and substrate [6] causing the different bindings present to resemble each other more.

4.6. Annealing experiments

In the annealing experiments the Ba covered Ag(111) crystal is flashed to elevated temperatures and subsequently cooled down. For all amounts of Ba present on the surface TDS gave no Ba desorption signal, thus the amount of Ba present on the surface remains constant during the annealing experiments. Because of the low sublimation temperature of Ag [27] the maximum temperature to which the crystal is flashed in the TDS experiments is about 820 K. The MEIS experiments also indicate that no Ba desorbs upon annealing. For Ba on W(110), desorption of Ba is only observed for temperatures above 1400 K [40], which indicates that the Ba forms a very strong bond with the substrate.

If less than a monolayer of Ba is present on the surface only small changes are observed in the WF and the recorded SEECC signal upon annealing. The observed XPS line widths, intensities and positions do not show any change within the experimental uncertainty. Apparently submonolayer coverages of Ba on Ag(111) are very stable and no large changes take place in the morphology and the electronic properties of the overlayer.

If, however, more than one monolayer (160 s dose or 0.6×10^{15} adsorbates cm^{-2}) Ba is adsorbed on the surface the stability of the overlayer is greatly reduced. As the temperature

is increased the WF shifts to lower values. Figure 10 shows a WF decrease of about 0.1 eV between 500 and 550 K and then even larger decrease between 620 and 820 K. For the amount of Ba present in figure 10 (400 s dose or 1.5×10^{15} adsorbates cm^{-2}) the final value obtained for the WF is as low as 1.9 ± 0.1 eV. This observation can be of great importance for the production rate of negative ions in proton Ba/Ag(111) scattering and other applications (see, e.g., [5]). In a first-order approximation the observed decrease in the WF will give rise to an increase in negative ion yield. However, we cannot exclude the possibility that the band structure of the system is affected such that the enhancement is masked [41]. Only future experiments measuring the negative ion yields produced can give an answer. Such studies are presently being performed in our institute [42].

Upon annealing the SEECC increases from -150 nA to $+10$ nA. Thus increase can be explained by the observed WF decrease which lowers the barrier for the electrons to escape into the vacuum.

By analysing the change in XPS line intensities and widths some clues about the effects causing the observed WF decrease can be obtained. As can be verified in figure 11, the Ba line intensity decreases while the Ag line intensity increases just at the temperature of the first WF decrease by 0.1 eV. The larger the amount of Ba present on the surface, the larger the observed difference in line intensity after annealing (cf. figure 12). For all coverages above 0.6×10^{15} adsorbates cm^{-2} the line intensities after the anneal are equal to the line intensities obtained after a dose of 300 s (1.1×10^{15} adsorbates cm^{-2}). The hypothesis that the apparent loss is due to desorbing Ba is in contradiction with the TDS experiments.

The changes in XPS line intensities and line widths can be explained by a change in morphology of the overlayer formed. From our adsorption study it is very likely that the overlayer formed at room temperature is initially relatively flat, although for the larger doses the formation of 3D clusters is possible. This results in a relatively high shielding of the substrate and thus a low substrate XPS signal. The adsorbate signal is expected to be large in such a flat overlayer since there is hardly any shielding of the adsorbate by the adsorbate itself [43]. If, however, the overlayer becomes more corrugated and high 3D structures are formed on the surface, a decrease in adsorbate signal will be observed since the self-shielding in the 3D structures is more important. In contrast, upon the formation of 3D clusters the substrate is less shielded, which will result in an increase in substrate signal. This is indeed what is observed in figure 11. In fact, as can be verified in figure 12, all the line intensities are equal to those obtained after a 300 s dose (1.1×10^{15} adsorbates cm^{-2}). This implies that for high coverages the clusters formed have to be large and high. The experimental results strongly suggest that the first Ba layer on top of the Ag(111) is not affected by the annealing. So, the line width of the Ag is not expected to change. At the transition temperature around 520 K the measured values for the Ba line width and the WF also become equal to those obtained after a 300 s dose (1.1×10^{15} adsorbed cm^{-2}). This again supports the idea that the clusters formed cover only a small part of the crystal and thus have to be rather high.

The formation of very large clusters is often observed [32] and arises through several stages of cluster growth. Most of the size increase occurs either through Ostwald ripening, i.e., the growth of larger clusters at the expense of smaller clusters due to the Gibbs–Thomson effect, or through coalescence when clusters merge upon contact. At room temperature clusters are not formed because the mobility of the adatoms is too low to attain the thermodynamically favoured configuration. Apparently for Ba on Ag(111), due to the low mobility of the adsorbate, a non-equilibrium overlayer is formed upon dosing at room temperature.

In a recent paper Bot *et al* [43] have shown that the observed changes in XPS signal for

the higher coverages can be quantitatively reproduced in a simple analytical model assuming a transition from an originally flat multilayer towards a more irregularly shaped or rough overlayer. In contrast to clusters formed by Ostwald ripening, the structures in this model are not very large and high. The structure obtained results from diffusive processes on a microscopic scale and is the structure giving rise to maximum entropy.

Other possible explanations for the observed intensity changes are the diffusion of Ba into the Ag bulk or the formation of an alloy. According to the phase diagram [29], diffusion into the bulk can be excluded. This is in agreement with Ba on W(011) [30] and the larger alkalis on Ag(111) [23]. Only Li shows some diffusion into the bulk. Although the phase diagram does not exclude the formation of an alloy, it seems very unlikely that alloy formation is only taking place for coverages above one monolayer. As already mentioned, no changes in the intensities are observed below one monolayer coverage.

The WF decrease and line width increase around 520 K can be explained by the same arguments as the changes in line intensities. However, the nature of the much larger WF decrease, which is accompanied by a further increase in line width, above 620 K is not known to us. Since no further changes in line intensities are observed above 550 K it is very likely that the overlayer is not changed in any way, although it is possible that some rearranging is taking place in the clusters. As on a clean Ag(111) crystal and on a crystal covered with less than a monolayer of Ba no similar WF differences are observed, it is very unlikely that the observed WF decrease is just an experimental artifact. Furthermore the observed reproducible WF decrease is supported also by the large increase in SEECC signal. In the dipole picture [6] for the adsorbate substrate binding in a flat overlayer all the individual dipoles depolarize each other. A possible explanation for the observed large WF decrease could be a kind of microscopic roughening of the surface which causes the depolarization of the individual dipoles to be less, but causes no changes of the observed line intensities.

4.7. Coadsorption with H_2

We will end this section by discussing briefly the coadsorption of Ba and H_2. In the experimental section it has already been mentioned that the H_2 does not stick on the Ag(111) crystal, which is in agreement with experimental results obtained by Yu *et al* [28]. Since upon annealing the morphology of the overlayer changes, the TDS results are obtained on preannealed samples. If H_2 is absorbed on a Ba covered crystal the sticking coefficient increases to about 10^{-4}. This value for the sticking coefficient does not change in our experiments for H_2 doses between 20 l and 400 l.

The very small WF decrease of 0.02 eV (for annealed as well as unannealed samples) and lack of change in XPS line intensities, positions and widths indicate that the effects on the morphology of the Ba/Ag(111) system are very minor. This is in agreement with similar experiments such as coadsorption of H_2 on Cs/W(110) [13].

The TDS experiments depicted in figure 14 indicate that there is only one peak present in the desorption spectrum, which shifts to lower temperatures as the amount of H_2 at the surface is increased. From this shift and from the symmetry of the peak it seems very likely that the experimental curves are the result of second-order kinetics [44]. This implies that the H_2 is dissociatively adsorbed to the surface. Dissociative adsorption of hydrogen is again in agreement with, e.g., the observations of Papageorgopoulos for H_2 on Cs/W(110) [13]. However, this author can identify two different binding states, which each give rise to a different desorption temperature. In our experiment we cannot exclude the existence of other binding states. If the desorption temperatures for the different binding states were almost the same it would be very hard to distinguish them solely by TDS experiments.

5. Summary

In this paper the adsorption of Ba on Ag(111) is studied by several techniques (AES, XPS, MEIS, SEECC, TDS and WF measurements). The experimental results show that initially a monolayer of Ba is formed. After the formation of the monolayer the growth changes. Most likely a structure is formed which resembles the structure formed by MSM growth or SK growth while the clusters are still rather small. The sticking coefficient is initially constant during the deposition of at least the first 1.8×10^{15} adsorbates cm^{-2}. From the attenuation of the electrons recorded in AES and XPS an IMFP of 11 ± 1 Å for 351 eV electrons and an IMFP of 17 ± 1 Å for 1113 and 1119 eV electrons is deduced.

Annealing a Ba covered crystal gives rise to interesting features. A crystal with less than one monolayer of Ba on top shows no changes in morphology and WF. However, the WF drops significantly in a two-step process when a crystal with more than one monolayer is annealed. The first WF decrease can be understood in terms of clustering of the overlayer. For the second (larger) WF decrease we have no adequate description.

Finally some coadsorption experiments with H_2 are performed that show that for all applied H_2 doses the sticking coefficient is constant. It is confirmed that the H_2 adsorbs dissociatively. From the TDS spectra one binding state could be identified.

Acknowledgments

The authors would like to thank A Raukema for his help in setting up the Auger measurements. Support for scientific exchange from NATO (contract CRG 900246) is gratefully acknowledged. This work is part of the research programme of the association agreement between the Stichting voor Fundamenteel Onderzoek der Materie (Foundation for Fundamental Research of Matter) and EURATOM and was made possible by financial support from the Nederlandse Organisatie voor Wetenschappelijk Onderzoek (Dutch Organization for the Advancement of Research) and EURATOM.

References

[1] Hopman H J and the NET Team 1988 *Proc. 3rd Euro. Conf. on the Production and Application of Light Negative Ions (Amersfoort 1988)* ed H J Hopman and W van Amersfoort (Amsterdam: FOM Institute) p 3

[2] See, e.g., Bacal M and Skinner D A 1990 *Comment. At. Mol. Phys.* **23** 283
Berlemont P, Skinner D A and Bacal M 1991 *Chem. Phys. Lett.* **183** 397

[3] See, e.g., van Os C F A, Heeren M A and van Amersfoort P W 1987 *Appl. Phys. Lett.* **51** 1495
Heeren R M A, Ćirić D, Hopman H J and Kleyn A W 1991 *Appl. Phys. Lett.* **59** 158 and references therein
Kleyn A W 1989 *AIP Conf. Proc.* **210** 3

[4] van Os C F A, van Amersfoort and Los J 1988 *J. Appl. Phys.* **64** 3863
van Os C F A 1989 *PhD Thesis* University of Utrecht

[5] See, e.g., Norman D, Tuck R A, Skinner H B, Wadsworth P J, Gardiner T M, Owen I W, Richardson C H and Thornton G 1987 *Phys. Rev. Lett.* **58** 519

[6] Gurney R W 1935 *Phys. Rev.* **47** 479

[7] Los J and Geerlings J J C 1990 *Phys. Rep.* **190** 133

[8] Argile C and Rhead G E 1989 *Surf. Sci. Rep.* **10** 277
Bauer E and Poppa H 1972 *Thin Solid Films* **12** 167

[9] Bauer E 1958 *Z. Kristallogr.* **110** 372

[10] Argile C and Rhead G E 1988 *Surf. Sci.* **203** 175

[11] Bonzel H P 1987 *Surf. Sci. Rep.* **8** 43

[12] See, e.g., Parker S D and Dobson P J 1986 *Surf. Sci.* **171** 267
[13] Papageorgopoulos C A 1989 *Phys. Rev.* B **40** 1546
[14] Reijnen P H F, van Slooten U, de Jongh A P, Kuijper J H M and Kleyn A W 1990 *Meas. Sci. Technol.* **1** 1244
Reijnen P H F 1990 *PhD Thesis* University of Amsterdam
[15] Wagner C D, Riggs W M, Davis L E, Moulder J F and Muilenberg G E 1979 *Handbook of X-ray Photoelectron Spectroscopy* ed G E Muilenberg (Minnesota: Perkin–Elmer Corporation)
[16] Marée P M J, de Jongh A P, Derks J W and van der Veen J F 1987 *Nucl. Instrum. Methods* B **28** 76
[17] Vrijmoeth J, Zagwijn P M, Frenken J W M and van der Veen J F 1991 *Phys. Rev. Lett.* **67** 1134
Zagwijn P M, Molenbroek A M, Vrijmoeth J, Ruwiel G J, Uiterlinden R M, ter Horst J, ter Beek J and Frenken J W M to be published
[18] van der Veen J F 1985 *Surf. Sci. Rep.* **5** 199
[19] Ziegler J F, Biersack J P and Littmark U 1985 *The Stopping and Ranges of Ions in Matter 1 The Stopping and Ranges of Ions in Solids* ed J F Ziegler (New York: Pergamon)
[20] van Loenen E J, Iwami M, Tromp R M and van der Veen J F 1984 *Surf. Sci.* **137** 1
[21] Seah M P and Dench W A 1979 *Surf. Interface Anal.* **1** 2
[22] Bartès-Labrousse M G and Rhead G E 1982 *Surf. Sci.* **116** 217
[23] Parker S D 1985 *Surf. Sci.* **157** 261
[24] Lamouri A and Krainsky I L 1992 *Surf. Sci.* **278** 286
[25] Lindgren S Å and Waldén L 1991 *Surf. Sci.* **257** L619
[26] Eyink K G, Lamartine B C, Lampert W V and Haas T W 1985 *Appl. Surf. Sci.* **20** 215
[27] Marbrow R A and Lambert R M 1976 *Surf. Sci.* **61** 317
[28] Yu C F, Whaley K B, Hogg C S and Siebener S J 1985 *J. Chem. Phys.* **83** 4217
[29] Bruzonne G, Ferretti M and Merlo F 1987 *J. Less-Common Met.* **128** 259
[30] Naumovets A G, Poplavsky V V and Vedula Yu S 1988 *Surf. Sci.* **200** 321
[31] Fedorus A G and Gonchar V V 1984 *Surf. Sci.* **140** 499
[32] Zinke-Allmang M, Feldman L C and Nakahara S 1990 *Kinetics of Ordering and Growth at Surfaces (NATO ASI Ser. B Physics 239)* ed M G Lagally (New York: Plenum) p 455
Zinke-Allmang M, Feldman L C and Grabow M H 1992 *Surf. Sci. Rep.* **16** 377
[33] Cotter M, Campbell S, Egdell R G and Mackrodt W C 1988 *Surf. Sci.* **197** 208
[34] Weijs P J M, Fuggle J C and van der Heide P A M 1992 *Surf. Sci.* **260** 97, 102
[35] Ishida H and Terakura K 1988 *Phys. Rev.*B **38** 5752
Johnson P D, Viescas A J, Nordlander P and Tully J C 1990 *Phys. Rev. Lett.* **64** 942
Schmalz A, Aminpirooz S, Becker L, Haase J, Neugebauer J, Scheffler M, Batchelor D R, Adams D L and Bøgh E 1991 *Phys. Rev. Lett.* **67** 2163
[36] Hollering R W J, Dijkkamp D, Lindelauf H W L, van der Heide P A M and Krijn M P C M 1990 *J. Vac. Sci. Technol.* **8** 3997
Vlachos D and Papageorgopoulos C A to be published
[37] 1971 *Handbook of Chemistry and Physics* 52nd edn (Cleveland, OH: Chemical Rubber Company)
[38] Fischer A, Krozer A and Schlapbach L 1992 *Surf. Sci.* **269/270** 737
[39] Ayyoob M and Hedge M S 1984 *J. Chem. Soc. Faraday Trans.* **1 80** 2703
[40] Miyake T and Yamamoto S 1993 *Surf. Sci.* **287/288** 340
[41] Teillet-Billy D and Gauyacq J P 1992 *Surf. Sci.* **269/270** 162
Barisov A G, Teillet-Billy D and Gauyacq J P 1992 *Surf. Sci.* **278** 99
[42] van Slooten U, Koppers W R, Teodoro O M N D, Kleyn A W, Los J, Teillet-Billy D and Gauyacq J P to be published
[43] Bot A, van Slooten U, Koppers W R and Kleyn A W 1993 *Surf. Sci.* **287/288** 901
[44] See, e.g., Woodruff D P and Delchar T A 1986 *Modern Techniques of Surface Science* (Cambridge: Cambridge University Press)